Mechanism and Machine Theory 44 (2009) 2164–2178

Contents lists available at ScienceDirect

Mechanism and Machine Theory

journal homepage: www.elsevier.com/locate/mechmt

Dynamics of highly elastic mechanisms using the generalized multiple shooting method: Simulations and experiments

Chao-Chieh Lan [a,*], Kok-Meng Lee [b], Jian-Hao Liou [a]

[a] Department of Mechanical Engineering, National Cheng Kung University, No. 1 University Road, Tainan 701, Taiwan
[b] Woodruff School of Mechanical Engineering, Georgia Institute of Technology, Atlanta, GA 30332-0405, United States

ARTICLE INFO

Article history:
Received 20 January 2009
Received in revised form 27 June 2009
Accepted 30 June 2009
Available online 11 August 2009

Keywords:
Elastic mechanisms
Flexible multibody dynamics
Shooting method
Hamilton's principle
Four-bar mechanism
Centrifugal stiffening

ABSTRACT

We present the generalized multiple shooting method (GMSM) to analyze the dynamics of elastic mechanisms. The GMSM solves a boundary value problem by treating it as an initial value problem. Its accuracy depends on the order of space marching schemes rather than size of discretization. Dynamic equations with joint boundary conditions are derived by using Hamilton's principle to be systematically solved by the GMSM. Comparing with existing solutions and experiments, the GMSM is shown to be efficient yet it captures deflection precisely. We expect it to serve as a good alternative to existing methods.

1. Introduction

Due to increasing requirements of compactness and high speed, dynamic analyses of elastic (flexible) mechanisms have been a subject of interest for simulation and control of modern machinery. Examples include space robot arms and high-speed robotic manipulators. Unlike nearly rigid body mechanisms where deformation is very small and does not affect mechanism behavior, the deformation of an elastic mechanism has great influence on its dynamics. Whether this type of deformation is intentionally designed [1–3] or unavoidable [4,5], the elastic part usually consists of slender, beam-like links. For this reason, classical beam dynamic models (Euler–Bernoulli or Timoshenko beam models) are usually applied. The models are satisfactory provided that a link undergoes a small deflection such that the assumption of a linear strain–displacement relation holds. However, for mechanisms involving highly elastic links [1–3], the models are unable to account for the effects of large deflection on the link motion. In order to predict more accurately the deflected shape during transient, there is a need for a model that captures the deflection of a highly elastic link.

With recent developments of finite element methods (FE), several types of FE formulations have been developed to analyze links undergoing large deflection and overall rotation. These formulations are broadly categorized by the choice of frames where link deformation and forces are described [6]. The *floating frame formulation* is based on defining deformation and forces relative to a floating frame which follows the rigid body motion of the link (for example, see Refs. [7,8]). This formulation makes use of linear FE theories since reliable FE packages are widely available. Although shear deformation can be further included, the link deflection is assumed to be small in order for the linear elasticity theory to hold. The *co-rotational frame formulation* defines deformation in a co-rotational frame and forces in the inertia frame. One of its original works was

* Corresponding author. Tel.: +886 6 2757575x62274; fax: +886 6 2352973.
E-mail address: cclan@mail.ncku.edu.tw (C.-C. Lan).

0094-114X/$ - see front matter © 2009 Elsevier Ltd. All rights reserved.
doi:10.1016/j.mechmachtheory.2009.06.006

presented by Rankin and Brogan [9] and has been applied to finite element software such as ANSYS®. It has been used to analyze many structural problems with large rotations. This formulation is independent of the element formulations used. Both the element and its nodes are attached to their own co-rotational frames. These frames are used to subtract the rigid body motion from the global displacement field to obtain the deformation of the element. Hsiao and Jang [10] extended the co-rotational formulation to analyze flexible planar linkages using a linear beam theory. Behdinan et al. [11] used the formulation to study planar beams undergoing large deflections. The *global frame formulation* defines both deformation and forces in the global frame. Simo and Vu-Quoc [12,13] were among the first to adopt this formulation. Later, Shabana [14] proposed the absolute nodal coordinate formulation and it has been an attracting method in recent years. This formulation has been extended to solve three-dimensional beam problems [15] and plate problems [16]. Compared with the floating frame formulation, the co-rotational and global frame formulations can handle links undergoing large deflection with large overall motion. However, Campanelli et al. [17] pointed out several restrictions of the co-rotational formulation for large deflection analysis. Specifically, the local rotation of end sections has to be less than 30° and small load steps have to be used. Other comparisons between the co-rotational formulation and the absolute nodal coordinate formulation are found in Ref. [17]. When modeling a mechanism with mixed elastic and rigid links, both co-rotational and global frame formulations treat rigid links in the same way as elastic links that require finite element meshes. They do not take advantages of rigid body properties and thus are computationally more costly than the floating frame formulation.

This paper proposes an alternative method based on the generalized multiple shooting method (GMSM) to analyze the dynamics of an elastic mechanism. Unlike the above finite element based methods, a shooting method solves a boundary value problem by treating it as an initial value problem. The generalized shooting method was introduced by Lan and Lee [18] to analyze large-deflected compliant mechanisms. This numerical method offers a simple formulation with higher order accuracy. This method was later extended as the generalized multiple shooting method to serve as the basis for shape design of compliant mechanisms [19]. While the GMSM has been demonstrated for static analysis, this paper builds upon Refs. [18,19] to explore the capability of analyzing dynamics of elastic mechanisms. The term elastic mechanism generally refers to a mechanism that consists of elastic links, where both revolute and clamped joints are included. A compliant mechanism can be regarded as its special case that mainly consists of clamped joints. Specifically, this paper begins by formulation of the GMSM. This is followed by a set of distributed-parameter governing equations to predict the motion of an elastic link. The equations precisely describe the kinematics of a transiently deformed link due to bending and axial deformation. For applications of an elastic mechanism, systematic procedures to derive joint boundary conditions are established. The Newmark scheme is then applied to discretize the dynamic equations so they can be further solved by the GMSM. Finally, comparisons with existing methods and experiments are given for verification.

2. Generalized multiple shooting method (GMSM)

Consider an ordinary differential equation (ODE) that governs the deflection of a link (for example, Euler–Bernoulli or Timoshenko beam equations). The ODE is recast as a set of normalized, first-order ODE of the following form:

$$\mathbf{q}' = \mathbf{f}(u, \mathbf{q}) \tag{1a}$$

where $\mathbf{q} = [\, q_1 \quad q_2 \quad \cdots \quad q_n \,]^T$ is a column of n variable functions, $0 \leqslant u \leqslant 1$ is an independent variable, and $\mathbf{q}' = d\mathbf{q}/du$. Next we consider an elastic mechanism that consists of ℓ links. Each link is governed by one set of Eq. (1a). We stack these equations as follows:

$$\begin{bmatrix} \mathbf{q}_1' \\ \vdots \\ \mathbf{q}_i' \\ \vdots \\ \mathbf{q}_\ell' \end{bmatrix} = \begin{bmatrix} \mathbf{f}_1(u, \mathbf{q}_1) \\ \vdots \\ \mathbf{f}_i(u, \mathbf{q}_i) \\ \vdots \\ \mathbf{f}_\ell(u, \mathbf{q}_\ell) \end{bmatrix} \tag{1b}$$

where subscript i denotes link number. The subscript i is also added to function $\mathbf{f}$ since each link may be generally governed by a different type of ODE. Since the links are connected together by various kinds of joints, these ℓ sets of first-order ODE's are coupled and must be simultaneously solved. To solve Eq. (1b) by the GMSM, we first divide the interval of integration [0 1] equally into N subintervals with $N+1$ nodes

$$0 = u_0 < u_1 < \cdots < u_j < \cdots < u_{N-1} < u_N = 1; \quad j = 0\text{—}N$$

The symbol u_j denotes the normalized arc length of the jth node. By doing this, Eq. (1b) is equally divided into N sub-ODE's. The form of each sub-ODE is identical to its original Eq. (1b) except that the span is now $u \in [\, u_j \quad u_{j+1} \,]$. Same as Eq. (1b), each sub-ODE requires a set of initial values in order to integrate the ODE in that subinterval. We denote the initial values of the jth sub-ODE as

$$\mathbf{q}(u_j) = [\, \mathbf{q}_1^T(u_j) \quad \ldots \quad \mathbf{q}_i^T(u_j) \quad \cdots \quad \mathbf{q}_\ell^T(u_j) \,]^T = [\, \boldsymbol{\mu}_{1j}^T \quad \ldots \quad \boldsymbol{\mu}_{ij}^T \quad \cdots \quad \boldsymbol{\mu}_{\ell j}^T \,]^T = \boldsymbol{\mu}_j; \quad j = 0\text{—}N-1$$

where $\boldsymbol{\mu}_j$ is an $\ell n \times 1$ vector. Since these initial values are not known in advance, we treat them as unknowns. For N sub-ODE's we have $\ell n \times N$ initial values

$$\boldsymbol{\mu} = [\,\boldsymbol{\mu}_0^T \quad \cdots \quad \boldsymbol{\mu}_j^T \quad \cdots \quad \boldsymbol{\mu}_{N-1}^T\,]^T$$

Hence there are totally ℓnN unknowns. These unknowns, depending on their physical model, are usually angles of rotation, displacements, or internal forces that characterize the geometry of a link. We then provide estimates to these unknowns in order to integrate each sub-ODE of Eq. (1b). After integration, the terminal values of the sub-ODE's must satisfy the corresponding equations as follows.

(i) ℓn terminal constraint equations that couple each set of Eq. (1b) together:

$$\mathbf{g}(\mathbf{q}(0), \mathbf{q}(1)) = 0 \tag{2a}$$

Eq. (2a) results from the joint boundary conditions that connect all the links together. Since a link is connected at its two ends, these equations are generally functions of $\mathbf{q}(0)$ and $\mathbf{q}(1)$. The number of terminal constraint equations must be equal to ℓn in order to be well-posed. An explicit formulation of Eq. (2a) will be provided in Section 3.2.

(ii) $(N-1)\ell n$ continuity equations that piece every sub-ODE of Eq. (1b) together:

$$\boldsymbol{\mu}_{j+1} = \mathbf{q}(u_{j+1}; \boldsymbol{\mu}_j); \quad j = 0\text{—}N-2 \tag{2b}$$

The vector $\boldsymbol{\mu}_j$ after the semicolon indicates that the value $\mathbf{q}(u_{j+1})$ is a function of the initial value $\boldsymbol{\mu}_j$ of the jth sub-ODE. Since each sub-ODE is part of a continuous ODE (Eq. (1b)), Eq. (2b) means that the values at the end of each sub-ODE must be equal to the initial values of the next sub-ODE. Note that for a more general formulation of the GMSM [19], additional unknown parameters and physical constraint equations are required.

We then begin an iterative process to find the solutions to the initial values so that after integration, the constraint and continuity equations in Eq. (2) are satisfied. Since the process is very similar to solving a system of nonlinear algebraic equations, methods such as Newton–Raphson or Quasi-Newton can be applied. For convenience of programming, the Jacobian matrix of Eq. (2) is approximated numerically. To further reduce the cost of Jacobian matrix computation, we adopt Quasi-Newton method that requires only one evaluation of the Jacobian matrix. On the other hand, the accuracy of the GMSM depends on the order of integration scheme used. For example, the result of using a fourth-order Runge–Kutta scheme is more accurate than that of a third-order scheme. However, the difference of computational cost between the third and fourth-order schemes is marginal (see Ref. [18] for detailed comparison). Hence a fourth-order scheme is usually applied.

For $N = 1$, Eq. (2b) vanishes and the GMSM reduces to generalized (single) shooting method (GSM). When integrating ODE's with complicated boundary conditions, solution profile due to poor estimates of initial values tends to go unbounded before the end of integration. To be able to iteratively correct the poor estimates, a shorter span of integration is necessary. Hence more than one subinterval ($N > 1$) are usually required to ensure convergence of the iterative process.

3. Dynamic model of a highly elastic mechanism

To analyze the motion of an elastic mechanism, we first derive a set of distributed-parameter equations for an elastic link. Boundary conditions at the joints of a mechanism are then formulated. Various types of joints are considered to include mechanisms of general configurations. The equations with boundary conditions are to be recast so they can be readily solved by using the GMSM. Advantages of the proposed model are also highlighted.

3.1. Dynamic equations governing an elastic link

Fig. 1 shows an initially straight link of length L in the global x–y frame. A non-dimensional arc length $u \in [0\ 1]$ is defined along the neutral axis of the link. To depict its deflected shape, we define ψ as the link deflection angle induced by bending.

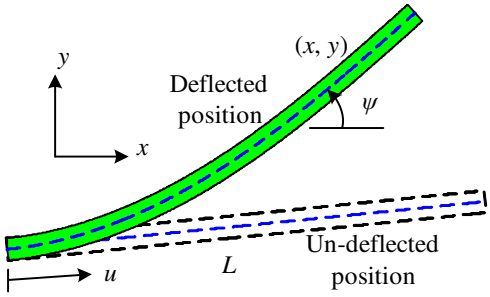

Fig. 1. Schematic of an elastic link.

The coordinate of a point on the neutral axis of the link is described by (x, y). The variables x, y, and ψ are functions of u and time t. They are expressed explicitly as $x(u, t)$, $y(u, t)$, and $\psi(u, t)$.

The total kinetic energy of the link is expressed as

$$K = \frac{L}{2}\int_0^1 [I_\rho \dot{\psi}^2 + A_\rho(\dot{x}^2 + \dot{y}^2)]du \tag{3}$$

where I_ρ is the mass moment of inertia per unit length, A_ρ is the mass per unit length, and a dot over a variable denotes the time derivative of that variable. Similarly, the potential (strain) energy of the link can be expressed as

$$V = \frac{1}{2L}\int_0^1 [EI(\psi')^2 + EA(e')^2]du \tag{4}$$

where I is the second moment of area, A is the cross section area, and E is the modulus of elasticity. The axial displacement e is measured along the neutral axis. A prime over a variable denotes the derivative with respect to the non-dimensional arc length u. The terms inside Eq. (4) represent the strain energy due to bending and axial deformations, respectively. Shear deformation is ignored here for clarity but it can be included in a similar fashion.

In practical applications, non-conservative forces applied on the link include external or internal dissipative forces. As an illustration, we adopt a linear viscous damping model so that at every point of the link, the point undergoes a drag force that is proportional in magnitude to the velocity of that point. The virtual work due to the drag force is formulated as

$$\delta W^{nc} = -L\int_0^1 (\sigma_1 \dot{x}\delta x + \sigma_2 \dot{y}\delta y)du \tag{5}$$

where σ_1 and σ_2 are the viscous damping coefficients in the x and y directions. In addition, the variables x, y, and ψ that appear in Eqs. (3)–(5) are not independent. They are related by the following two geometric constraints

$$g_1 = x' - (L + e')\cos\psi = 0; \quad g_2 = y' - (L + e')\sin\psi = 0 \tag{6a, b}$$

With Eqs. (3)–(5), (6a), (b), the equations of motion of the elastic link can be derived by using Hamilton's principle, where the following variational form holds

$$\int_{t_1}^{t_2}\left(\delta K - \delta V + \delta W^{nc} - \int_0^1 (h\delta g_1 + v\delta g_2)du\right)dt = 0 \tag{7}$$

The integration limits t_1 and t_2 are two arbitrary instants of time. The introduced variables h and v are the Lagrange multipliers for Eqs. (6a,b), respectively. With them, we have enough (six) variables for the variational procedure. The resulting partial differential equations that govern the dynamics of a large-deflected link are written as follows

$$\frac{EI}{L^2}\psi'' - I_\rho\ddot{\psi} + v\left(\frac{e'}{L} + 1\right)\cos\psi - h\left(\frac{e'}{L} + 1\right)\sin\psi = 0 \tag{8a}$$

$$L(A_\rho\ddot{x} + \sigma_1\dot{x}) - h' = 0; \quad L(A_\rho\ddot{y} + \sigma_2\dot{y}) - v' = 0 \tag{8b,c}$$

$$x' - (L + e')\cos\psi = 0; \quad y' - (L + e')\sin\psi = 0 \tag{8d,e}$$

$$EAe'' - L(h\cos\psi + v\sin\psi)' = 0 \tag{8f}$$

Eq. (8a) is the moment balance equation. The rotational inertia term $I_\rho\ddot{\psi}$ is often very small (due to I_ρ) and may be neglected in practical applications. Eqs. (8b,c) are the results of applying Newton's second law to each infinitesimal segment directly. From observing Eqs. (8a,b,c), the Lagrange multipliers h and v turn out to be the internal forces acting on an infinitesimal segment in the positive x and y directions. To further include the effect of gravity in practical applications, the term $-LA_\rho g$ should be added to Eq. (8c) for a gravitational force, for example, in the positive y direction. Eqs. (8d,e) are the same geometric constraints as Eqs. (6a,b). They must be solved simultaneously with the rest of Eq. (8). Compared with linear beam theories that are based on the assumption of small deflection, Eqs. (8d,e) provide exact kinematic description for the neutral axis of a deflected beam even for very large transient deflections. Eq. (8f) is the force balance equation in the axial direction. For many applications the axial displacements are small and may be ignored for convenience.

For an elastic mechanism that consists of multiple links, each link is governed by one set of Eq. (8). The displacement functions of all links are described expediently in the same x–y frame (or global frame). Without unnecessary intermediate or local frames, coordinate transformations can be avoided. This is in contrast to the floating frame or co-rotational frame formulations that are based on a frame attached to each link. Since deformation and internal forces are described in the global frame, the model provided here may be considered as a type of the global frame formulation.

3.2. Boundary conditions at the joints

Eq. (8) that governs the dynamics of a link is subjected to various types of boundary conditions. For an elastic mechanism, those conditions appear at joints where the ends of links are connected. Mathematically, the boundary conditions can be expressed as terminal constraint (algebraic) equations that must be valid for all time. Without loss of generality, exclusive

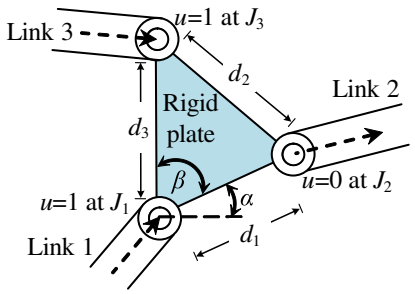

Fig. 2. Schematic of a rigid plate that connects three elastic links.

revolute and clamped joints are investigated. We first consider a movable rigid plate that connects three links shown in Fig. 2. A free body diagram of the plate yields force balance equations as follows

$$h_1(1) - h_2(0) + h_3(1) = 0; \quad v_1(1) - v_2(0) + v_3(1) = 0 \tag{9a}$$

Whether the sign of the force is positive or negative depends on how the direction of the non-dimensional arc length u is (arbitrarily) defined for each link. For example, Link 1 ends at J_1 with $u = 1$ and hence $h_1(1)$ has a positive sign. Link 2 starts at J_2 with $u = 0$ and hence $h_2(0)$ has a negative sign. For each of the three links, external forces also produce axial displacements. Since e is defined along the positive direction of non-dimensional arc length u, its initial value is zero and increases with increasing u. At $u = 1$, the internal axial force has to balance with external forces. Thus the boundary conditions of axial displacements depend on the value of u at the joints

$$e(0) = 0 \quad \text{or } EAe'(1) - L(h\cos\psi + v\sin\psi)|_{u=1} = 0 \tag{9b}$$

In addition to forces, the displacements of the three joints have to match at the rigid plate

$$\begin{aligned} &x_2(0) - x_1(1) = d_1\cos\alpha; \quad y_2(0) - y_1(1) = d_1\sin\alpha \\ &x_3(1) - x_1(1) = d_3\cos(\alpha+\beta); \quad y_3(1) - y_1(1) = d_3\sin(\alpha+\beta) \end{aligned} \tag{9c}$$

The parameters d_1–d_3 are the distances between the centers of joints J_1–J_3. For clamped joints, the angle $\alpha = \psi_1(1) + \text{constant}$. For revolute joints, the angle α is solved by the following moment balance equation at J_1

$$[v_2(0)d_1\cos\alpha - h_2(0)d_1\sin\alpha] - [v_3(1)d_3\cos(\alpha+\beta) - h_3(1)d_3\sin(\alpha+\beta)] = 0$$

Depending on whether they are clamped or revolute joints, the corresponding moment/angle conditions are

$$\begin{aligned} &(EI_1/L_1)\psi_1'(1) - (EI_2/L_2)\psi_2'(0) + (EI_3/L_3)\psi_3'(1) - [v_2(0)d_1\cos\alpha - h_2(0)d_1\sin\alpha] + [v_3(1)d_3\cos(\alpha+\beta) \\ &\quad - h_3(1)d_3\sin(\alpha+\beta)] = 0 \end{aligned} \tag{9d}$$

Clamped:

$$\psi_2(0) - \psi_1(1) = \text{const.}; \quad \psi_3(1) - \psi_1(1) = \text{const.} \tag{9e}$$

Revolute:

$$\psi_1'(1) = 0; \quad \psi_2'(0) = 0; \quad \psi_3'(1) = 0 \tag{9f}$$

Eq. (9d) is the moment balance equation at J_1, where the sign convention is the same as that in Eq. (9a). Eq. (9e) states that the angle differences from Link 1 to Link 2 and Link 3 are the same before and after deformation. Eq. (9f) states that a revolute joint cannot resist moments and thus the derivative of ψ has to be zero for all the three links. Observing Eqs. (9d)–(9f) both clamped and revolute joints include three constraint equations. Regardless of clamped or revolute, the rigid plate in Fig. 2 has a total of 12 constraint equations. From above we may deduce that a general movable rigid plate that connects m links should have $4m$ terminal constraint equations. The extensions of Eq. (9) to more than (or less than) three links are rather straightforward. In an elastic mechanism, we can treat a certain (massless) link as a rigid plate when its flexural rigidity is much larger than others. In this way, the solution procedure is more computationally efficient since the deformation of the rigid plate does not have to be accounted for. In the extreme case when the size of a plate shown in Fig. 2 is very small, the three joints coincide as shown in Fig. 3. Eq. (9) then reduces to a simpler version by nullifying the terms involving the distances d_1–d_3.

Fig. 4 illustrates three other joint types. The ground-fixed joint in Fig. 4a may be subject to either a torque input M or angle input φ. The free joint in Fig. 4b may be subject to external force F_x or F_y. Fig. 4c shows a guided joint with a massless slider block. The corresponding moment/angle and force/displacement boundary conditions are listed in Table 1. Each joint in Table 1 has four constraint equations regardless of its type.

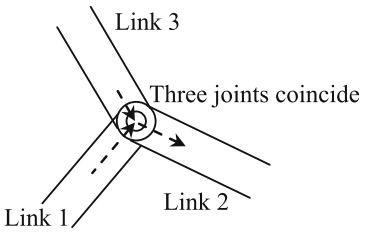

Fig. 3. Special case of Fig. 2.

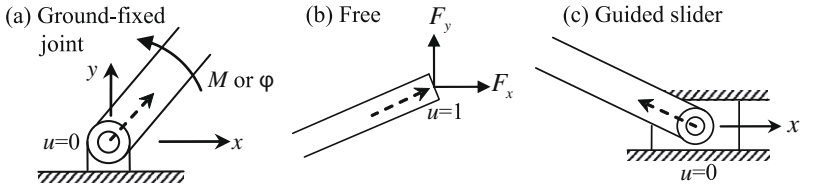

Fig. 4. Types of joints and boundary conditions.

When Eq. (8) is recast into the form of Eq. (1a) with $n = 8$, Eq. (9) and the constraint equations in Table 1 serve as the terminal constraint equations in Eq. (2a). For the differential equations to be well-posed, the number of terminal constraint equations has to be equal to 8ℓ for an elastic mechanism with ℓ links. The formulation of continuity equations (Eq. (2b)) will be given in Section 4.

4. Temporal approximations

Eq. (8) with terminal constraint equations formulated in Section 3.2 is a system of nonlinear hyperbolic equations. We adopt, but are not limited to, the Newmark family of integration schemes to temporally discretize Eq. (8) so that the spatial domain can be further solved by using the GMSM. The Newmark scheme is an implicit method that finds the current displacement using equations of motion at current time. Consider the x position of a particular point on a link. Let the position x^k, its velocity $\dot{x}^k$, and acceleration $\ddot{x}^k$ denote the approximate solution to $x(t^k, u)$, $\dot{x}(t^k, u)$, and $\ddot{x}(t^k, u)$ at time instant t^k, respectively. When at time t^k the solutions of x^k, $\dot{x}^k$, and $\ddot{x}^k$ have been obtained, the Newmark scheme approximates the velocity and acceleration at the next time instant t^{k+1} by using the following formulas:

$$\ddot{x}^{k+1} = (2/a_2\Delta t^2)(x^{k+1} - x^k) - (2/a_2\Delta t)\dot{x}^k - (1/a_2 - 1)\ddot{x}^k \tag{10a}$$

$$\dot{x}^{k+1} = \dot{x}^k + (1 - a_1)\Delta t\ddot{x}^k + a_1\Delta t\ddot{x}^{k+1} \tag{10b}$$

where $\Delta t = t^{k+1} - t^k$ denotes the time step size and (a_1, a_2) are Newmark parameters that determine the stability and accuracy of the scheme. By applying Eq. (10a) to the terms involving time derivatives, Eq. (8) can be written as a system of time-independent ordinary differential equations involving unknown functions ψ^{k+1}, h^{k+1}, v^{k+1}, x^{k+1}, y^{k+1}, and e^{k+1} to be solved. To apply the GMSM, we further recast the equations into a set of first-order ODE as follows. For clarity of expression we neglect the rotational inertia term in Eq. (8a) and damping terms in Eqs. (8b,c).

$$\mathbf{q}' = \begin{bmatrix} \psi^{k+1} \\ (\psi')^{k+1} \\ h^{k+1} \\ v^{k+1} \\ x^{k+1} \\ y^{k+1} \\ e^{k+1} \\ (e')^{k+1} \end{bmatrix}' = \begin{bmatrix} (\psi')^{k+1} \\ -L/EI[(e')^{k+1} + L](v^{k+1}\cos\psi^{k+1} - h^{k+1}\sin\psi^{k+1}) \\ LA_\rho[(2/a_2\Delta t^2)(x^{k+1} - x^k) - (2/a_2\Delta t)\dot{x}^k - (1/a_2 - 1)\ddot{x}^k] \\ LA_\rho[(2/a_2\Delta t^2)(y^{k+1} - y^k) - (2/a_2\Delta t)\dot{y}^k - (1/a_2 - 1)\ddot{y}^k] \\ [L + (e')^{k+1}]\cos\psi^{k+1} \\ [L + (e')^{k+1}]\sin\psi^{k+1} \\ (e')^{k+1} \\ L/EA(h^{k+1}\cos\psi^{k+1} + v^{k+1}\sin\psi^{k+1})' \end{bmatrix} \tag{11}$$

Eq. (11) is then solved by the GMSM presented in Section 2 to obtain the solution at time step $k + 1$. Specifically, the spatial domain is divided into N subintervals so that the unknown initial values of each sub-ODE are expressed as

$$\boldsymbol{\mu}_j^{k+1} = [\,\psi^{k+1} \quad (\psi')^{k+1} \quad h^{k+1} \quad v^{k+1} \quad x^{k+1} \quad y^{k+1} \quad e^{k+1} \quad (e')^{k+1}\,]^T|_{u=u_j}; \quad j = 0\text{–}N-1$$

Table 1
Constraint equations at various joints.

	Moment and angle	Force and displacement
Fixed	$\begin{cases}\psi'(0)+(L/EI)M=0 & \text{moment input}\\ \psi(0)=\varphi & \text{angle input}\\ \psi(0)=\text{constant} & \text{clamped}\end{cases}$	$x(0)=0;\ y(0)=0;\ e(0)=0$
Free	$\psi'(1)=0$	$h(1)-F_x=0;\ v(1)-F_y=0;\ e'(1)=0$
Guided	$\psi'(0)=0$	$h(0)=0;\ y(0)=0;\ e(0)=0$

For a mechanism with ℓ links, there are $8N\ell$ unknown initial values. The matching terminal constraint equations are formulated in Section 3.2. For cases of multiple shooting ($N>1$), continuity equations are further required to piece each sub-ODE together

$$\boldsymbol{\mu}_{j+1}^{k+1}=\mathbf{q}(u_{j+1};\boldsymbol{\mu}_j^{k+1});\quad j=0\text{—}N-2$$

After solving time step $k+1$, the approximate functions $(\dot{\psi}^{k+1},\ddot{\psi}^{k+1})$, $(\dot{x}^{k+1},\ddot{x}^{k+1})$, and $(\dot{y}^{k+1},\ddot{y}^{k+1})$ are computed by using Eq. (10). They are plugged into Eq. (11) again to solve for the next time step $k+2$. Although we need to estimate the initial values $\boldsymbol{\mu}$ for each time step, we may use the solved initial values from the previous time step as estimates to the initial values of the current step. Hence we only need to offer estimates for the very first time step.

Note that to begin the iterative calculation of Eq. (11), information of the initial conditions $(\psi^0,\dot{\psi}^0,\ddot{\psi}^0)$, $(x^0,\dot{x}^0,\ddot{x}^0)$ and $(y^0,\dot{y}^0,\ddot{y}^0)$ is required. The initial positions and velocities will be given and the initial accelerations can be obtained by assuming zero applied force at $t=0$:

$$\ddot{\psi}^0=(EI/L^2I_\rho)(\psi'')^0;\quad \ddot{x}^0=0;\quad \ddot{y}^0=0 \tag{12}$$

The first initial acceleration in Eq. (12) is not required if the rotational inertia term in Eq. (8a) is neglected.

5. Illustrative examples

We verify our proposed method by four examples. Example 1 demonstrates the GMSM for analyzing a shear deformable beam. Example 2 simulates the motion of a high-speed rotating link and compares the results of using the GMSM with those previously published. Example 3 studies the dynamics of an elastic slider crank mechanism using two different types of material. Finally, a four-bar mechanism is presented in Example 4 to validate the GMSM experimentally. Except for Example 1, the other three examples use the link dynamic equations (Eqs. (8)–(9)) established in Section 3. We use intervals $N=20$, time step size $\Delta t=0.005$ s, and Newmark parameters $(a_1,a_2)=(0.5,0.5)$ for these three examples. A fourth-order Runge–Kutta method with step size $d=0.005$ is applied as the space marching scheme. Note that for closed-loop mechanisms the link axial deformation is very small and can be neglected to reduce computation complexity. By doing so, the revised governing equations remove Eq. (8f), Eq. (9b), and the terms involving e and e' in Eqs. (8a)–(8e) and Table 1. The recast state-space form has $n=6$ variable functions with 6ℓ terminal constraint equations and $6\ell(N-1)$continuity equations. Example 2 and Examples 3–4 illustrate the analyses with and without considering axial deformation, respectively.

Solving these examples requires four steps: (i) recast the ODE in a state-space form as Eq. (1), (ii) formulate unknown initial values $\boldsymbol{\mu}$ and terminal constraint equations $\mathbf{g}$, (iii) temporally discretize the ODE and then divide it into sub-ODE's to obtain continuity equations, and (iv) provide first estimates of $\boldsymbol{\mu}$ to iteratively integrate the ODE until the terminal constraint equations and continuity equations are satisfied. Due to the systematic procedure, the only difference among these examples is step (ii), which will be detailed in each example.

5.1. Example 1: Effect of shear deformation

The GMSM itself is generic and can be used to solve various boundary value equations. We apply this method to solve Timoshenko's beam equations, which take into account shear deformation in addition to flexural deformation. Timoshenko's beam equations (linear) are

$$\frac{d}{dx}\left[\kappa GA\left(\frac{dw}{dx}-\psi\right)\right]+f(x)=0;\quad EI\frac{d^2\psi}{dx^2}+\kappa GA\left(\frac{dw}{dx}-\psi\right)=0 \tag{13a}$$

where x is the axial coordinate of the beam, w is the transverse deflection of the beam, $f(x)$ is the transversely distributed load function, G is the shear modulus, and κ is the shear correction factor. When a beam is clamped at $x=0$ and free at $x=L$, the known terminal constraint equations are

$$w=0 \text{ and } \psi=0 \text{ at } \underline{x=0};\quad d\psi/dx=0 \text{ and } \kappa GA\left(\frac{dw}{dx}-\psi\right)=F \text{ at } \underline{x=L} \tag{13b}$$

where F is the concentrated load applied at $x=L$. For constant f, the exact solutions to Eq. (13) are

$$w = \frac{0.5fL^2 + FL}{2EI}x^2 - \frac{F + fL}{6EI}x^3 + \frac{f}{24EI}x^4 + \frac{(F + fL)x - 0.5fx^2}{\kappa GA}; \quad \psi = \frac{0.5fL^2 + FL}{EI}x - \frac{F + fL}{2EI}x^2 + \frac{f}{6EI}x^3 \tag{14}$$

To solve Eq. (13) by using the GMSM with $N = 1$, we introduce new variables $q_1 = w$, $q_2 = dw/dx$, $q_3 = \psi$, and $q_4 = d\psi/dx$ so they can be expressed as the following set of first-order ODE

$$[\,q_1' \quad q_2' \quad q_3' \quad q_4'\,]^T = [\,q_2 \quad q_4 - \tfrac{f}{\kappa GA} \quad q_4 \quad \tfrac{\kappa GA}{EI}(q_3 - q_2)\,]^T$$

The unknown initial values and terminal constraint equations are

$$\boldsymbol{\mu} = [\,q_1(0) \quad q_2(0) \quad q_3(0) \quad q_4(0)\,]^T \quad \text{and} \quad \mathbf{g} = [\,q_1(0) \quad q_3(0) \quad q_4(L) \quad \kappa GA(q_2(L) - q_3(L)) - F\,]^T = 0.$$

Hence the initial values can be solved by iteratively satisfying the terminal constraint equations. For comparison, we solve Eq. (13) again by using the finite element methods. However, care must be taken for the element-wise interpolation of variables w and ψ in order not to yield trivial solutions ($w = \psi = 0$), which is termed as shear-locking [20]. Reduced integration elements (RIE) and consistent interpolation elements (CIE) were developed to solve Eq. (13) without exhibiting shear-locking. As an illustration, we solve Eq. (13) by using RIE (linear interpolation). The transverse deflection w's computed by using GMSM (which is naturally free of shear-locking) and RIE are then compared in Fig. 5 with exact solutions in Eq. (14). A beam with square cross section is used with material properties provided in Fig. 5. RIE uses 10, 20, and 50 elements while the GMSM uses ode23 and ode45 solver in Matlab®. The solver ode23 refers to Runge–Kutta formulas of a second and third-order pair while ode45 refers to a fourth and fifth-order pair. It can be seen that RIE requires at least 50 elements to achieve the order of accuracy of the results of GMSM using ode23. The result of using ode45 is almost the same as the exact solution.

5.2. Example 2: A high-speed rotating link

Applications of a high-speed rotating link can be found in helicopter blades, flexible robotic manipulators, and turbine blades. As mentioned in Ref. [6], the floating frame formulation is restricted to simulate motion of links with moderate angular velocities. For high-speed rotating links the centrifugal force stiffens the link (known as centrifugal stiffening effect or geometric stiffening effect). It has been shown that the floating frame formulation fails to capture this effect and thus causes numerical instability. The instability is due to its assumption of linear strain–displacement relations, which neglects the coupled longitudinal and transverse displacements caused by bending deformation [21]. Methods [22,23] have been proposed for the floating frame formulation to solve this problem. Since the coupled displacements are described by Eq. (8), we demonstrate using this example that the GMSM can naturally simulate a high-speed rotating link without further modifications. Consider a straight link attached to a hub shown in Fig. 6. The unknown initial values are $\boldsymbol{\mu}_j = [\,\psi \quad \psi' \quad h \quad v \quad x \quad y \quad e \quad e'\,]^T|_{u=u_j} (j = 0\text{—}N-1)$ with terminal constraint equations as follows

$$\begin{aligned} &\text{At } J_1 : \mathbf{g} = [\psi(0) - \varphi; \quad x(0); \quad y(0); \quad e(0); \\ &\text{At } J_2 : \qquad \psi'(1); \quad h(1); \quad v(1); \quad e'(1)] = 0 \end{aligned} \tag{15}$$

where the angle input φ at the hub (J_1) is given as follows

$$\varphi(t) = \begin{cases} \omega_s/T_s\{t^2/2 + (T_s/2\pi)^2[\cos(2\pi t/T_s) - 1]\} & t < T_s \\ \omega_s(t - T_s/2) & t \geqslant T_s \end{cases}$$

Two benchmark cases were previously performed [13,22–24] to examine whether instability occurs when simulating a high-speed rotating link. We use the GMSM to simulate the two cases for verification. Table 2 shows the parameters for the two

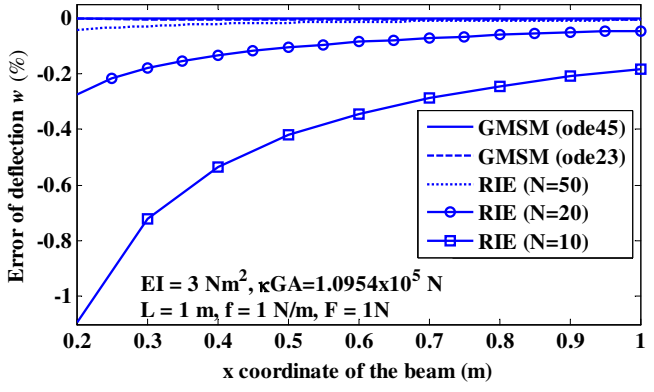

Fig. 5. Error comparisons of GMSM and RIE.

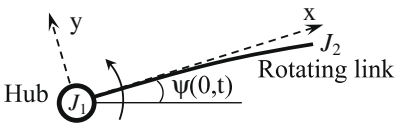

Fig. 6. A high-speed rotating link.

Table 2
Simulation parameters for the spinning link.

Simulation Parameters	Case 1 [22,24]	Case 2 [13,23]
Length of link L	8 m	10 m
Density ρ	2766.67 kg/m^3	3000 kg/m^3
Moment of inertia I	8.214×10^{-9} m^4	1.997×10^{-7} m^4
Cross-sectional area A	7.299×10^{-5} m^2	4×10^{-4} m^2
Young's Modulus E	6.895×10^{10} Pa	7×10^{10} Pa
(T_s, ω_s)	(15 s, 2 rad/s)	(15 s, 6 rad/s)

cases. For Case 1, Fig. 7 shows the tip displacement in the local x direction. As the link rotates very fast, its axial displacement due to centrifugal forces becomes obvious. After $t \geqslant T_s$, the tip experiences a steady-state axial extension 2.7385×10^{-5} m. Fig. 8 shows the tip deflection in the local y direction. When the long beam starts with a very high acceleration, it will deflect and the maximal tip deflection is $y = -0.280$ m at $t = 7.0$ s (agrees with Ref. [22] where $y = -0.282$ m). Table 3 compares the computed tip steady-state axial extension of using the GMSM with those published [13,24]. Both cases are considered and matched, with maximal difference 0.03%.

5.3. Example 3: Dynamics of an elastic slider crank mechanism

Fig. 9 shows a slider crank mechanism driven by an input torque M at revolute joint J_1. Link 1 (crankshaft) connects to Link 2 (connecting rod) through revolute joint J_2. Link 2 is tied to another massless slider through revolute joint J_3. The slider moves smoothly in the x direction, which resembles the configuration in Fig. 4c. The arrows inside the links indicate positive directions of u. The unknown initial values of the mechanism are $\boldsymbol{\mu}_{ij} = [\psi_i \quad \psi_i' \quad h_i \quad v_i \quad x_i \quad y_i]^T|_{u=u_j} \quad (i = 1\text{—}2,\ j = 0\text{—}N-1)$ with terminal constraint equations formulated as follows

$$\begin{aligned} &\text{At } J_1: \mathbf{g} = [EI_1\psi_1'(0)/L_1 + M; \quad x_1(0); \quad y_1(0); \\ &\text{At } J_2: \quad \psi_1'(1); \quad \psi_2'(1); \quad h_1(1) + h_2(1); \quad v_1(1) + v_2(1); \quad x_1(1) - x_2(1); \quad y_1(1) - y_2(1); \\ &\text{At } J_3: \quad \psi_2'(0); \quad h_2(0); \quad y_2(0)] = 0 \end{aligned} \tag{16}$$

where the input torque M is given as follows and simulation parameters in Table 4

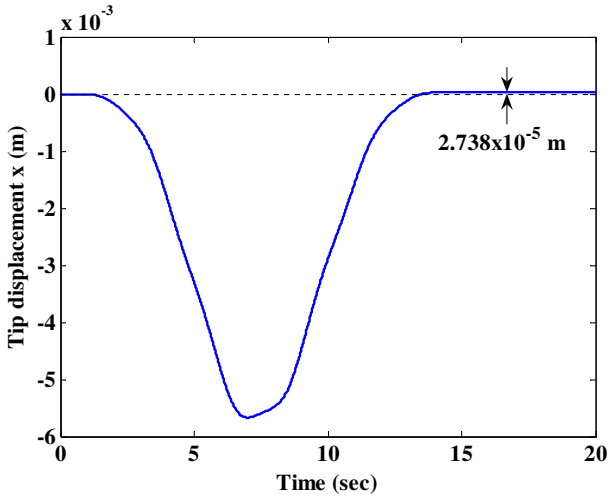

Fig. 7. Displacement of the tip in the local x direction (Case 1).

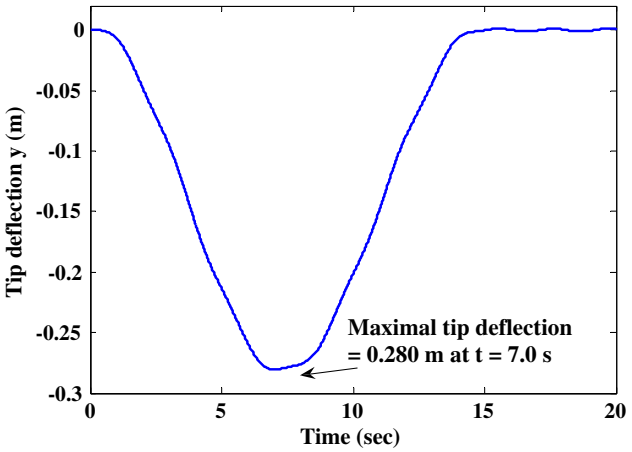

Fig. 8. Deflection of the tip in the local y direction (Case 1).

Table 3
Steady-state axial extension of the tip.

	Case 1	Case 2
Previously published results	2.7393×10^{-5} m [24]	5.14×10^{-4} m [13]
Results computed by using the GMSM	2.7385×10^{-5} m	5.14×10^{-4} m

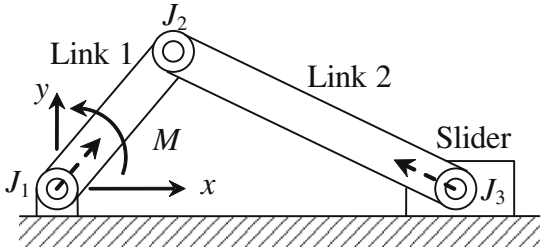

Fig. 9. Elastic slider crank mechanism.

$$M(t) = \begin{cases} 0.01 \sin\left(\frac{\pi}{1.2}t\right) & 0 \leqslant t < 1.2 \\ 0 & 1.2 \leqslant t \end{cases}$$

Under the above geometry and loading conditions, we select two different materials, aluminum (E = 70 GPa, ρ = 2710 kg/m^3) and rubber (E = 3 MPa, ρ = 2550 kg/m^3), to perform simulation using the GMSM and the co-rotational method (implemented in ANSYS®). In the ANSYS simulation, BEAM4 and COMBIN7 elements are used to model the flexible links and revolute joints, respectively. Fig. 10 shows the simulated slider block displacements using the two methods. Maximal difference is less than 0.3%. The rubber slider crank mechanism deflects more due to its compliance. The energy profile with respect to time is compared in Fig. 11. The results obtained by the GMSM and ANSYS show very good agreement. Since there is no input work after t = 1.2 s, the overall energy (kinetic plus strain energy) remains unchanged. Although the energy profile looks very much the same in Fig. 11, there is a small oscillation in the results of the co-rotational method, as can be seen in the enlarged view in Fig. 12. More time steps, larger mesh size, or more significant digits, do not improve the results.

Table 4
Simulation parameters for the elastic slider crank

Simulation Parameters	Values
Length of link (L_1, L_2)	(0.2, 0.4) m
Moment of inertia (I_1, I_2)	$(4.350 \times 10^{-10}, 4.350 \times 10^{-10})$ m^4
Cross section area (A_1, A_2)	$(7.225 \times 10^{-5}, 7.225 \times 10^{-5})$ m^2
Initial tip location	$[x_1(1), y_1(1)] = [0.2, 0]$ m; $[x_2(1), y_2(1)] = [0.6, 0]$ m

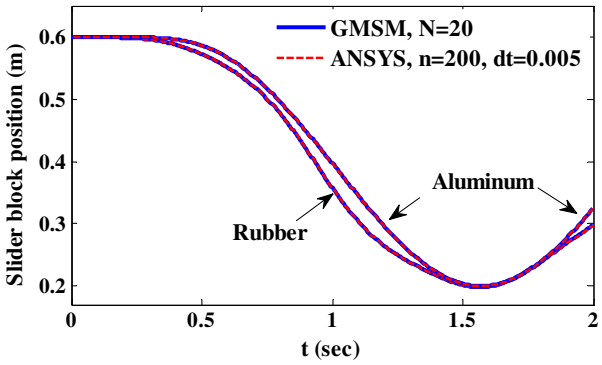

Fig. 10. Horizontal displacement of the slider block.

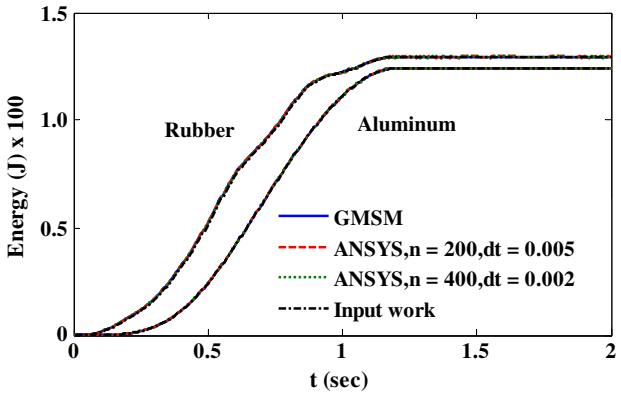

Fig. 11. Energy balance of the slider crank mechanism.

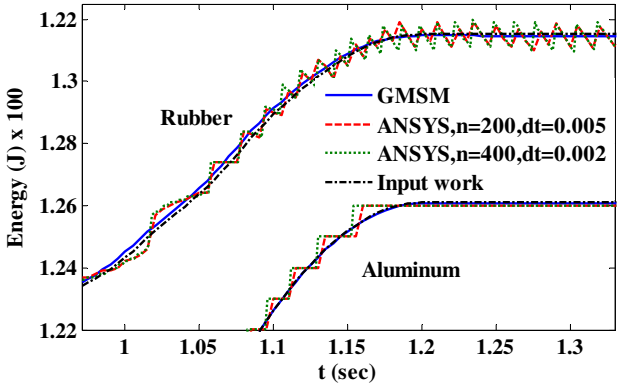

Fig. 12. Locally enlarged view of Fig. 11.

Table 5 compares the computation time of using the co-rotational method and the GMSM in a Pentium 4 computer (3.40GHz CPU with 2GB RAM). For fairness, the time step size and spatial discretization size of both methods are chosen to be the same. As can be seen, the computation time of using the co-rotational method is more than four times that of the GMSM. The improvement of computation time may be explained by the following: The accuracy of FE based methods is usually determined by the mesh size and thus the number of nonlinear equations to be solved. On the other hand, the accuracy of the GMSM depends on the order of space marching schemes. The number of nonlinear equations to be solved for the GMSM is determined by subinterval number *N*. More subintervals mainly improve convergence rather than accuracy. Hence the number of nonlinear equations to be solved for the GMSM is usually much less than that of FE methods. Since the

Table 5
Comparison of computation time for Example 3.

	Aluminum	Rubber
Co-rotational method (n = 200, Δt = 0.005 s, ANSYS)	234.08 s	229.25 s
GMSM (d = 0.005, Δt = 0.005 s, MATLAB)	44.61 s	49.16 s

computation time is primarily determined by the number of nonlinear equations to be solved, the GMSM can as a result be more efficient.

5.4. Example 4: An elastic four-bar mechanism

To validate the GMSM for analyzing large-deflected mechanisms, we perform an experiment using an elastic four-bar mechanism. Previously published experiments focused on the overall displacement of a vibrating cantilever [25] or lightly elastic four-bar mechanisms [26,27]. Experiments on a highly elastic four-bar mechanism, to the best of the author's knowledge, have not been found in the literature. Fig. 13 shows a schematic and detailed dimensions of a highly elastic four-bar mechanism. Two aluminum square brackets rigidly connect three spring steel beams at J_2 and J_3 so they form a rectangle. The three beams are denoted as Links 1, 2 and 3. The arrows beside the beams indicate positive directions of u. The beam flexural rigidities are determined from cantilever vibration experiments. The brackets are much thicker than the three beams and thus are considered rigid. The boundary conditions (Eqs. (9c)–(9e)) at a rigid plate can be applied here to accurately account for the bracket geometry. For clarity, the negligible mass and geometry of the brackets are not considered. Hence the unknown initial values are $\boldsymbol{\mu}_{ij} = [\,\psi_i \quad \psi_i' \quad h_i \quad v_i \quad x_i \quad y_i\,]^T|_{u=u_j}$ $(i = 1\text{—}3,\ j = 0\text{—}N-1)$ with terminal constraint equations formulated as follows

$$
\begin{aligned}
&\text{At } J_1: \mathbf{g} = [\psi_1(0) - \pi/2;\ x_1(0);\ y_1(0)\\
&\text{At } J_2: \quad \psi_1(1) - \psi_2(0) - \frac{\pi}{2};\ \frac{EI_1}{L_1}\psi_1'(1) - \frac{EI_2}{L_2}\psi_2'(0);\ h_1(1) - h_2(0);\ v_1(1) - v_2(0);\ x_1(1) - x_2(0);\ y_1(1) - y_2(0);\\
&\text{At } J_3: \quad \psi_2(1) - \psi_3(0) - \frac{\pi}{2};\ \frac{EI_2}{L_2}\psi_2'(1) - \frac{EI_3}{L_3}\psi_3'(0);\ h_2(1) - h_3(0);\ v_2(1) - v_3(0);\ x_2(1) - x_3(0);\ y_2(1) - y_3(0);\\
&\text{At } J_4: \quad \psi_3(1) + \frac{\pi}{2};\ x_3(1) - L_2;\ y_3(1)\Big] = 0
\end{aligned}
\tag{17}
$$

To test for large deflection, J_3 is given an initially displacement Δ = 11.0 cm in the positive x direction and then released. Fig. 14 shows the experiment setup, where a high-speed camera (250 fps, 640 × 480 pixels) is used for motion capture. A transient deformed position is shown in Fig. 15. The x displacement of midpoint B with respect to time is recorded in Fig. 16. By comparison, we see that the result of GMSM agrees well with that from the experiment. The differences at the peaks can be explained by the fact that we ignore actual aerodynamic damping in the GMSM simulation. Since the four-bar mechanism with aerodynamics damping can be regarded as a very lightly damped system, the difference between the experiment and the GMSM will not be distinguishable until several periods of vibration. To show the longitudinally shortened displacement due to bending of Links 1 and 3, we record the y displacement of Point B. This y displacement, though small compared to the x displacement, increases with increasing transverse deflection of Links 1 and 3. Fig. 17 shows the agreement of the experiment with the GMSM result. The GMSM is able to predict this displacement because deformation is described along the neutral axis of a link with aid of Eqs. (8d,e). Other existing models, which may be linear (for example, Euler–Bernoulli) or nonlinear describing deformation along the original position of a link, are unable to capture displacement in the y direction. In other words, when simulating using those models, the y displacement of point B would be identically zero.

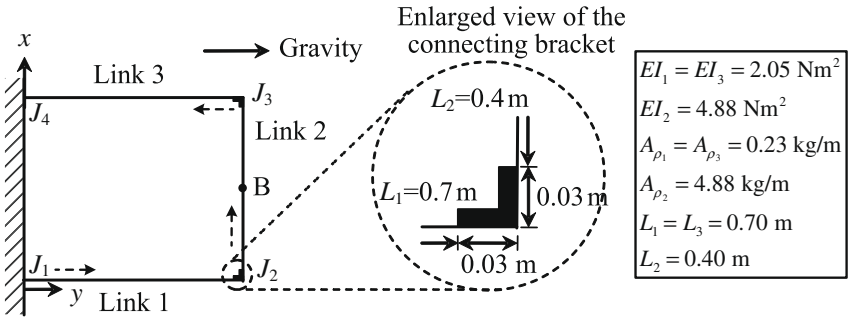

Fig. 13. Schematic of an elastic four-bar mechanism.

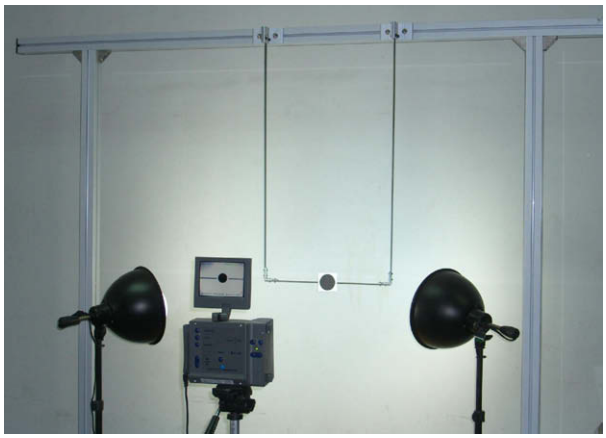

Fig. 14. Experiment setup.

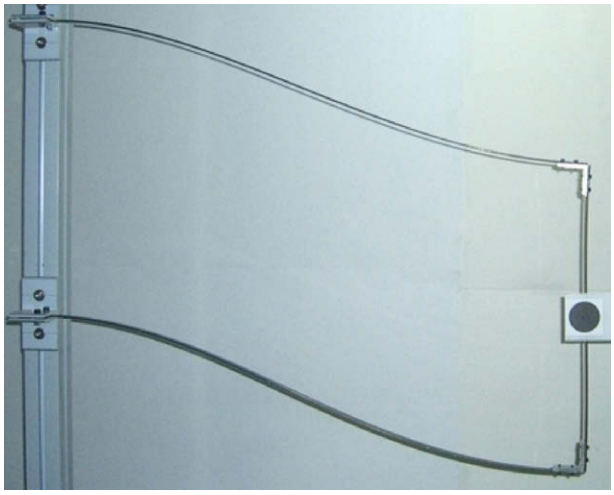

Fig. 15. Transient deformation.

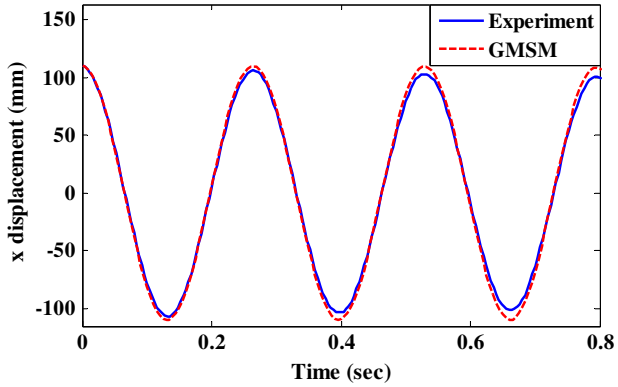

Fig. 16. Comparison of x displacement (Point B).

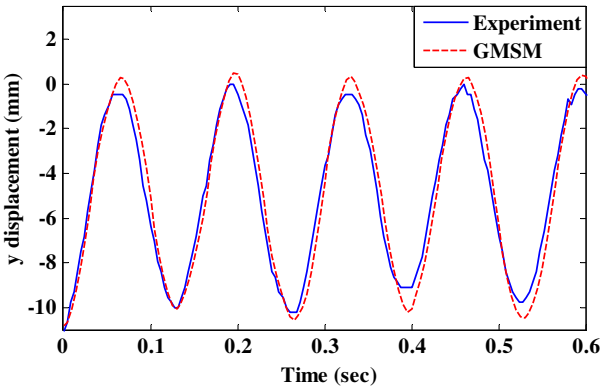

Fig. 17. Comparison of y displacement (Point B).

6. Conclusions

We present the generalized multiple shooting method (GMSM) for analysing the dynamics of an elastic mechanism. While the GMSM can be applied to any type (both linear and nonlinear) of differential equations, a set of governing equations is derived in Section 3 to effectively describe the exact kinematics of a large-deflected beam. We further offer a systematic formulation to model clamped, revolute, and sliding joints so that the necessary boundary conditions of mechanisms can be generated. The computational complexity primarily depends on the number of elastic links (ℓ). In many applications, axial deformation is ignored and hence the number of terminal constraint equations is 6ℓ.

Through four illustrative examples, the GMSM has been demonstrated to be a computationally efficient method with rather convenient formulation. Twenty subintervals ($N = 20$) are shown to be sufficient for simulating a highly elastic link. To reduce the computation cost for analyzing relatively stiff links, ten subintervals are satisfactory. For static analysis such as Example 1, only one or two subintervals are required. Experimental comparisons of using an elastic four-bar mechanism have also shown that the method can accurately predict the lateral displacement of the coupler caused by large-deflected motion. This type of displacement, though very small, cannot be ignored when precision motion is required. Since the GMSM is shown to be generic, its extension to spatial mechanisms is straightforward given three-dimensional beam differential equations. We expect that the GMSM presented here provides a very good alternative to existing methods for analyzing serial or parallel mechanisms where the effect of link flexibility on their dynamics is a concern.

Acknowledgement

Financial support of the National Science Council of Taiwan (NSC95-2218-E006-035) is greatly appreciated.

References

[1] K.-M. Lee, Design criteria for developing an automated live-bird transfer system, IEEE Trans. Rob. Autom. 17 (4) (2001) 483–490.
[2] Cameron Boyle, L.L. Howell, S.P. Magleby, M.S. Evans, Dynamic modelling of constant-force compression mechanisms, Mech. Mach. Theory 38 (12) (2003) 1469–1487.
[3] X. Wang, J.K. Mills, Dynamic modelling of a flexible-link planar parallel platform using a substructuring approach, Mech. Mach. Theory 41 (6) (2006) 671–687.
[4] M. Osinski, A. Maczynski, S. Wojciech, The influence of ship motion in regular waves on the dynamics of an offshore crane, Arch. Mech. Eng. 2 (2004) 131–163.
[5] A. Izadbakhsh, J. McPhee, S. Birkett, Dynamic modeling and experimental testing of a piano action mechanism with a flexible hammer shank, ASME J. Comput. Nonlinear Dyn. 3 (2008) 031004.
[6] T.M. Wasfy, A.K. Noor, Computational strategies for flexible multibody systems, ASME Appl. Mech. Rev. 56 (6) (2003) 553–613.
[7] R.A. Laskin, P.W. Likins, R.W. Longman, Dynamical equations of a free–free beam subject to large overall motions, J. Astronaut. Sci. 31 (4) (1983) 507–528.
[8] W.J. Book, Recursive Lagrangian dynamics of a flexible manipulator arm, Int. J. Robot. Res. 3 (1984) 87–101.
[9] C.C. Rankin, F.A. Brogan, An element independent corotational procedure for the treatment of large rotations, ASME J. Press. Vessel Technol. 108 (1986) 165–174.
[10] K.M. Hsiao, J.Y. Jang, Dynamic analysis of planar flexible mechanism by co-rotational formulation, Comput. Methods Appl. Mech. Eng. 87 (1991) 1–14.
[11] K. Behdinan, M.C. Stylianou, B. Tabarrok, Co-rotational dynamic analysis of flexible beams, Comput. Methods Appl. Mech. Eng. 154 (1998) 151–161.
[12] J.C. Simo, L. Vu-Quoc, On the dynamics of flexible beams under large overall motions–The plane case: Part I, ASME J. Appl. Mech. 53 (1986) 849–854.
[13] J.C. Simo, L. Vu-Quoc, On the dynamics of flexible beams under large overall motions–The plane case: Part II, ASME J. Appl. Mech. 53 (1986) 855–863.
[14] A.A. Shabana, Dynamics of Multibody Systems, Wiley, N.Y., 1998.
[15] A.A. Shabana, R.Y. Yakoub, Three dimensional absolute nodal coordinate formulation for beam elements: theory, ASME J. Mech. Des. 123 (4) (2001) 606–613.
[16] A.M. Mikkola, A.A. Shabana, A New Plate element Based on the Absolute Nodal Coordinate Formulation, ASME DETC, Pittsburgh, PA, 2001.
[17] M. Campanelli, M. Berzeri, A.A. Shabana, Performance of the incremental and non-incremental finite element formulations in flexible multibody problems, ASME J. Mech. Des. 122 (4) (2000) 498–507.

[18] C.-C. Lan, K.-M. Lee, Generalized shooting method for analyzing compliant mechanisms with curved members, ASME J. Mech. Des. 128 (4) (2006) 765–775.
[19] C.-C. Lan, Y.-J. Cheng, Distributed shape optimization of compliant mechanisms using intrinsic functions, ASME J. Mech. Des. 130 (2008) 072304.
[20] R.N. Reddy, An Introduction to the Finite Element Method, McGraw-Hill, NY, 1993.
[21] T.R. Kane, R.R. Ryan, A.K. Banerjee, Dynamics of a cantilever beam attached to a moving base, AIAA J. Guid., Control, Dyn. 10 (2) (1987) 139–151.
[22] S.-C. Wu, E.J. Haug, Geometric non-linear substructuring for dynamics of flexible mechanical systems, Int. J. Numer. Methods Eng. 26 (1988) 2211–2226.
[23] O. Wallrapp, R. Schwertassek, Representation of geometric stiffening in multibody system simulation, Int. J. Numer. Methods Eng. 32 (1991) 1833–1850.
[24] K.E. Dufva, J.T. Sopanen, A.M. Mikkola, A two-dimensional shear deformable beam element based on the absolute nodal coordinate formulation, J. Sound Vib. 280 (3–5) (2005) 467–1165.
[25] W.-S. Yoo, J.-H. Lee, S.-J. Park, J.-H. Sohn, O. Dmitrochenko, D. Pogorelov, Large oscillations of a thin cantilever beam: physical experiments and simulation using the absolute nodal coordinate formulation, Nonlinear Dyn. 34 (2003) 3–29.
[26] F.W. Liou, A.G. Erdman, Analysis of a high-speed flexible four-bar linkage: Part II –Analytical and experimental results on the Apollo, ASME J. Vibrat. Acoust. Stress Reliab. Des. 111 (1) (1989) 42–47.
[27] A. Gasparetto, On the modeling of flexible-link planar mechanisms: experimental validation of an accurate dynamic model, ASME J. Dyn. Syst. Meas. Control 126 (2) (2004) 365–375.